New Journal of Physics
The open access journal for physics

Density-dependent tunneling in the extended Bose–Hubbard model

Michał Maik[1,2], Philipp Hauke[2,3], Omjyoti Dutta[1,2], Maciej Lewenstein[2,4] and Jakub Zakrzewski[1,5,6]

[1] Instytut Fizyki imienia Mariana Smoluchowskiego, Uniwersytet Jagielloński, ulica Reymonta 4, PL-30-059 Kraków, Poland
[2] ICFO—Institut de Ciències Fotòniques, Mediterranean Technology Park, E-08860 Castelldefels, Barcelona, Spain
[3] Institute for Quantum Optics and Quantum Information of the Austrian Academy of Sciences, A-6020 Innsbruck, Austria
[4] ICREA—Institució Catalana de Recerca i Estudis Avançats, E-08010 Barcelona, Spain
[5] Mark Kac Complex Systems Research Center, Uniwersytet Jagielloński, Kraków, Poland
E-mail: jakub.zakrzewski@uj.edu.pl

New Journal of Physics **15** (2013) 113041 (14pp)
Received 26 June 2013
Published 20 November 2013
Online at http://www.njp.org/
doi:10.1088/1367-2630/15/11/113041

Abstract. Recently, it has become apparent that when the interactions between polar molecules in optical lattices become strong, the conventional description using the extended Hubbard model has to be modified by additional terms, in particular a density-dependent tunneling term. We investigate here the influence of this term on the ground-state phase diagrams of the two-dimensional extended Bose–Hubbard model. Using quantum Monte Carlo simulations, we investigate the changes of the superfluid, supersolid and phase-separated parameter regions in the phase diagram of the system. By studying the interplay of the density-dependent hopping with the usual on-site interaction U and nearest-neighbor repulsion V, we show that the ground-state phase diagrams differ significantly from those expected from the standard extended Bose–Hubbard model.

[6] Author to whom any correspondence should be addressed.

Contents

1. Introduction

In the last decade, the physics of ultra-cold atoms in optical lattice potentials has undergone extensive developments due to the extreme controllability and versatility of the realizable many-body systems (for recent reviews see [1, 2]). The tight-binding description predicted in 1998 [3], termed Bose–Hubbard model (BHM) for bosonic atoms with contact s-wave interactions, was soon after verified via the experimental observation of the superfluid (SF)–(MI) transition [4]. For particles interacting via a long-range (e.g. dipole–dipole) potential, the original model has to be modified, typically including a density–density interaction between different sites. The simplest approximation, taking into account only the interaction between nearest neighbors, is termed the extended BHM (EBHM). As compared to the BHM, the extended model allows for the existence of novel quantum phases such as checkerboard solids, supersolid (SS) phases [5–10], exotic Haldane insulators [11] and more.

Recently, however, it has been realized that even in the simpler case of contact s-wave interactions, in certain parameter regimes, carefully performed tight-binding approximations lead to an additional correlated tunneling term in the resulting microscopic description. This term, known in the case of fermions as bond-charge contribution [12], is even more important for bosons [13–16]. It is found that such tunneling terms, along with the effect of higher bands, can provide an explanation [14, 17] for the unexpected shift in the MI–SF transition point for Bose–Fermi [18, 19] and Bose–Bose mixtures [20] as well as shifts in absorption spectra for bosons in optical lattices [15].

One may expect that similar bond-charge (or density-dependent tunneling) effects may also play an important role in the presence of dipolar interactions. This assumption has been verified by some of us [21] in a recent study, where it has been shown that the additional terms in the Hamiltonian may destroy some insulating phases and may create novel pair-SF states. That study [21] has been restricted to a one-dimensional (1D) model due to the numerical methods used. Here, we use quantum Monte Carlo (QMC) methods to study softcore dipolar gases trapped in two-dimensional (2D) square optical lattices, where we assume a tight confinement in the remaining z direction (which is also the polarization direction of the dipoles). A similar 2D model, without the density-dependent tunneling terms, was analyzed before [8], providing us with a benchmark against which we may test the importance of density-dependent tunneling. In [8], an SS phase was observed in the EBHM at half filling. Such an SS is characterized by the coexistence of SF and crystal-like density–density diagonal long-range order [5–10].

Experimental evidence of this counter-intuitive quantum phase is still missing, since the claim of an experimental realization of supersolidity in ^{4}He [22, 23] could not be reproduced in later experiments [24, 25]. As we shall see, in the present model, the sign of the additional tunneling (or, more precisely, the relative sign between the standard tunneling and the density-dependent one) can stabilize or destabilize the SS phase.

2. The model

The appropriate tight-binding model, for studying interacting dipolar bosons occupying the lowest band in a lattice, reads [21]

$$H = -t\sum_{\langle i,j\rangle}(a_i^\dagger a_j + \text{h.c.}) + \frac{U}{2}\sum_i n_i(n_i-1) + V\sum_{\langle i,j\rangle} n_i n_j$$
$$- T\sum_{\langle i,j\rangle}(a_i^\dagger(n_i+n_j)a_j + \text{h.c.}) + P\sum_{\langle i,j\rangle}(a_i^\dagger a_i^\dagger a_j a_j + \text{h.c.}) - \mu\sum_i n_i, \qquad (1)$$

where $a_i^\dagger$ (a_i) is the creation (annihilation) operator of a boson at site i and n_i is the number operators; t is the regular hopping term; U the onsite repulsion; and μ the chemical potential. We assume a system of dipolar bosons in a 2D square lattice with dipolar moments polarized perpendicularly to the lattice, thus leading to dipole–dipole repulsion. Then, the present model contains three terms that come from the dipolar interactions, the nearest-neighbor repulsion V, the density-dependent hopping T and the correlated pair tunneling P. We restrict here the range of V to the nearest neighbors to allow for a direct comparison with the results of Sengupta *et al* [8] and Sowiński *et al* [21]. Within the standard EBHM, both the T and P terms are neglected. However, the analysis presented in [21] has shown that although V is typically an order of magnitude larger than both T and P, the latter terms cannot be neglected in the presence of strong dipolar interactions.

The four parameters U, V, T and P have the same physical origin, namely interactions, and are therefore correlated. However, in the 2D model, changing the trapping frequency in the direction perpendicular to the plane affects quite strongly only the on-site U term (for dipolar as well as for the contact part of the interactions). Thus, we shall consider U as an independent parameter. To facilitate a comparison with earlier works (e.g. [8]) that did not take T tunneling into account, we span a similar parameter range for U, V and filling fractions. The values of T, V and P are strongly correlated as they originate from nearest-neighbor scattering due to long-range interactions. For a broad range of optical lattice depths, the parameters T and V are typically related as $V \approx |10T|$. The absolute value of P is almost another magnitude smaller than T (compare figure 1 of [21]). Thus, for simplicity, we will set $V = |10T|$ in the following and neglect the P term altogether. This will allow us to study in depth the effects due to density-dependent tunnelings. The previous study [21] has shown that there is a broad tunability regarding the relationship of the two tunneling parameters T and t, allowing a regime where the two hopping terms have opposite signs and even the exotic situation that T dominates over t. For example, for weak trapping frequency along the polarization direction, t and T have opposite signs and for strong trapping frequency t and T have the same signs. Thus, for possible experimental realizations of polar bosons [26, 27], one can reach the two limits of bond-charge tunneling by tuning the trapping potential along the polarization direction [21].

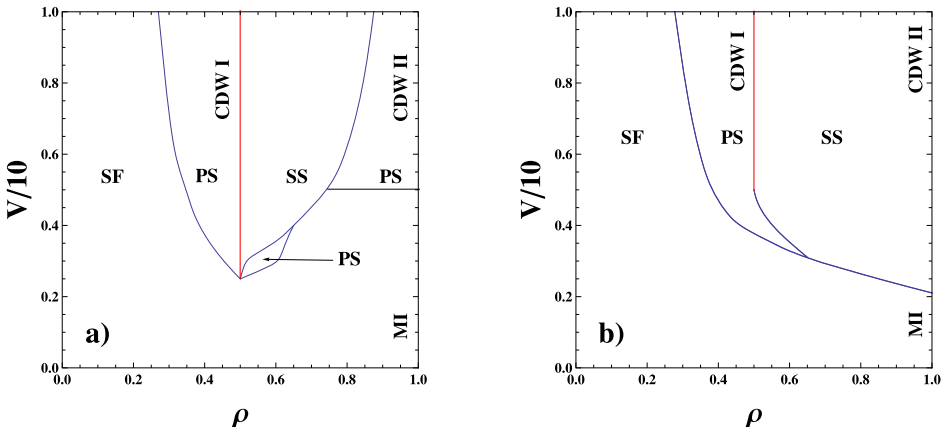

Figure 1. The phase diagram in the $\rho - V$ parameter space without density-dependent tunneling term, $T = 0$, for (a) $U = 20$ and (b) $U = 5$. The energy unit is $t = 1$. Panel (a) reproduces the results of [8]. The model contains various phases. The red solid line indicates the CDW (CDW I) at half filling; other phases present are the SF, SS and at unit filling either MI or another CDW (CDW II); PS denotes phase separated regions. When the on-site interaction becomes weaker, as shown in panel (b), the SS phase becomes larger and PS regions disappear at fillings larger than $1/2$.

Whether both the hopping terms are of the same or opposite signs has a major influence on the phases that will appear in the system. Generally speaking, when both the hopping terms have the same sign, one can expect an increase in the influence of the overall hopping. Otherwise, if the signs are opposite, there will be a competition between the two terms. Therefore, the influence of the additional density-dependent hopping can be expected to strongly affect the phase diagram.

To form an intuition about our system, let us give a brief summary of the results from the previous study [21] of a similar 1D system with both a density-dependent and a pair-hopping term. In that study, exact diagonalization (system sizes between $L = 8$ and 16) and the multiscale entanglement renormalization ansatz (system sizes up to $L = 128$) were used to study the phase diagram at zero temperature. The results, when both T and P are set to zero, show the existence of three phases. At weak interaction, there is an SF phase, while at stronger dipolar strength, two charge density wave (CDW) phases appear. The CDW phases are characterized by a periodic, crystal-like structure where occupied and empty sites alternate in a checkerboard pattern. In the following, we denote cases where the populated sites are occupied by a single atom (two atoms) as CDW I (II). In the 1D case of [21], the two observed CDW phases are a CDW I phase at half filling with a modulation of $|\ldots 010101\ldots\rangle$ and a CDW II phase at unit filling with a modulation of $|\ldots 020202\ldots\rangle$. Now, when the extra terms T and P are incorporated into the Hamiltonian, besides an overall deformation of the phase diagram, there appears also a novel pair-SF (PSF) phase. This more exotic phase is characterized by a finite two-particle NN correlation function $\Phi_i = \sum_{\{j\}} \langle a_j^\dagger a_j^\dagger a_i a_i \rangle$ and a smaller non-vanishing one-particle correlation function $\phi_i = \sum_{\{j\}} \langle a_j^\dagger a_i \rangle$. On the other hand, no SS phase has been observed in [21]. In the present study of a 2D lattice, on the contrary, we do observe an SS behavior, but we do not find any indications for the existence of a PSF phase.

2.1. Considered observables

In the analysis of Hamiltonian (1), we employ the stochastic series expansion (SSE) code, a QMC algorithm from the Algorithms and Libraries for Physics Simulations (ALPS) project [28]. We mainly rely on three observables. First, we study the density, $\rho = \langle n_i \rangle$, as a function of the chemical potential. Plateaus in the corresponding graphs indicate insulating phases, such as MI or CDW phases. The employed variant of QMC works in the grand-canonical ensemble, i.e. at fixed chemical potential. Discontinuous jumps in the density as a function of chemical potential signify regions of phase separation (PS) in the canonical phase diagrams. Namely, when the filling is fixed to a value which is not stable at any chemical potential, the system acquires the required filling only in the mean, by forming domain walls between two phases that are thermodynamically stable.

To distinguish not only different insulating phases (MI, CDW I and CDW II) but also the SF and the SS phases, we consider two other observables. These are the structure factor and the SF stiffness, both of which we analyze as functions of density. The structure factor is defined as

$$S(\mathbf{Q}) = \left\langle \left| \sum_{i=1}^{N} n_i \, \mathrm{e}^{\imath \mathbf{Q} \mathbf{r}_i} \right|^2 \right\rangle / N^2. \tag{2}$$

Here, N denotes the number of lattice sites and we focus on the wave vector $\mathbf{Q} = (\pi, \pi)$, which corresponds to a checkerboard modulation pattern. This observable has a peak when the particles are arranged in either of the CDW phases. This will help to distinguish the MI phase from the CDW phase, which cannot be done from the density graphs alone. For example, when a system is at unit filling, the structure factor is finite in the CDW II state, whereas it vanishes in the usual MI state.

The other observable is the SF stiffness, which can be calculated from the winding numbers of the QMC code. It is defined as

$$\rho_{\mathrm{s}} = \frac{\langle W^2 \rangle}{4\beta}, \tag{3}$$

where W is the winding-number fluctuation of the world lines and β is the inverse temperature (in this study $\beta = 20$). This value shows what per cent of the system is in an SF state. Taking SF stiffness and structure factor together, we can also identify the SS phase. The SS phase occurs when both SF stiffness and structure factor are non-zero. Note that since the PS regions do not correspond to stable grand-canonical phases as computed in the SSE QMC code, we cannot assign any values of observables for them. This is not necessary, however, since PS regions are already unambiguously identified by jumps in plots of density against chemical potential.

From these three observables (density, structure factor and SF stiffness), we are now able to distinguish the most prominent phases that we are looking for. These observables cannot, however, identify PSF phases, the signature of which is, as mentioned previously, a non-vanishing two-particle NN correlation function Φ_i. In its current version, the QMC code provided in the ALPS library is not able to calculate these correlation functions. In order to extract this observable, the code would have to be written with a two-headed worm, which could then be analyzed in a similar way as the SF stiffness, but with the difference that the winding numbers would represent the flowing of pairs instead of single particles [29]. Fortunately, one can identify a dominant PSF order parameter using a different technique, namely by studying

the density histograms of the QMC code. If these histograms show only even values of particles instead of a uniform distribution, this means that the bosons always pair up, indicating PSF behavior [29].

3. Ground-state phase diagrams

In this section, we present our QMC results for the ground-state phase diagram of Hamiltonian (1). We focus on a 2D square lattice with linear system sizes ranging from $L = 8$ to 16 (where $N = L \times L$). We observe a fast convergence of the results with L, similar to [8]. Therefore, the considered system sizes suffice, especially since we are interested not in the precise determination of phase boundaries, but in the global qualitative changes in the phase diagrams, which—as we will see—can be quite drastic. We present phase diagrams at two different values of the on-site repulsion ($U = 20$ and 5) for varying density and T (and therefore for varying V, since $V = 10|T|$). The two U values are chosen in such a way that we can compare nearly hardcore behavior, achieved at $U = 20$, with softcore behavior, for $U = 5$. Up to four bosons are allowed per site for both the cases, which seems sufficient for densities below unit filling (we tested in some instances against maximal occupation of six bosons per site). Further, at $U = 20$ we can compare our data with known results of the usual EBHM, which was studied thoroughly in [8]. We compare phase diagrams obtained with and without density-dependent tunnelings. For simplicity and ease of comparison to [8], we restrict our study to unit filling or less. Furthermore, for a more detailed evaluation of these phase diagrams, we study a few cuts at representative parameter values.

3.1. Phase diagrams at vanishing density-dependent tunneling

We begin our analysis with phase diagrams of the regular EBHM, illustrated in figure 1. This provides an overview of the behavior of the considered systems under a more common Hamiltonian, which does not have a density-dependent term T. We consider the case of strong repulsion $U = 20$, discussed previously in [8], as well as softer interacting bosons with $U = 5$.

3.1.1. Phase diagram at strong on-site repulsion ($U = 20$). For ease of comparison and for later reference, figure 1(a) reproduces the phase diagram of $U = 20$ that has been thoroughly investigated in [8]. It is well known that for $\rho < \frac{1}{2}$, there exist only two distinct regions, the SF phase and a PS region. For sufficiently low values of V, the system stays SF across the entire density range until unit filling, where it becomes an MI state. At half filling, a CDW I phase appears at a critical value of V, which in the present case lies around $V = 2.5$. A system in a checkerboard phase (CDW I) can be doped by holes or particles. When it is doped with holes, these create domain walls and cause the system to phase separate, preventing the appearance of an SS phase. In the case of hardcore bosons, this behavior would be mirrored for $\rho > \frac{1}{2}$, due to particle–hole symmetry. In the case of softcore bosons, such particle–hole symmetry can break down. At sufficiently low V, a region of PS appears and the system does present a hardcore-like behavior, but as the NN repulsion is increased, this PS region disappears. Since now the particles can occupy either an empty or occupied site, it is no longer necessary for the domain walls to form and the system can move into an SS state. Moreover, at a certain value of V, upon increasing ρ the SS phase is followed by a region of PS, instead of going into an SF phase and then becoming an MI. At unit filling, this PS region then changes to the CDW II phase, which

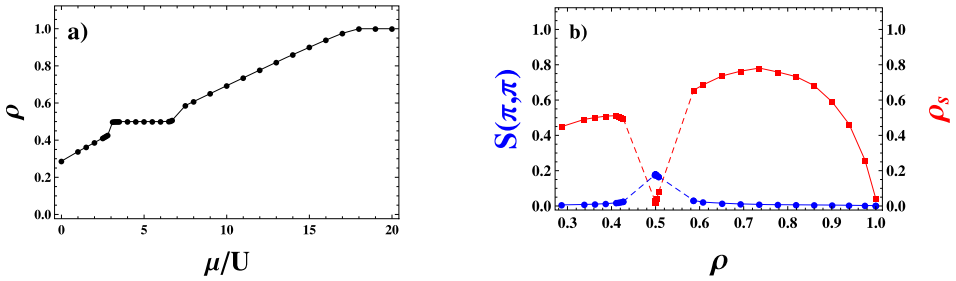

Figure 2. Identification of different phases as exemplified for $U = 20$ and $V = 3.0$ based on the density in (a) as well as the structure factor (blue circles) and the SF stiffness (red squares) shown versus density in (b). Plateaus in ρ as a function of μ indicate incompressible crystal phases. Jumps denote PS (the densities that are jumped over do not correspond to thermodynamically stable phases). Moreover, a finite SF stiffness characterizes an SF phase and a finite structure factor a CDW order. When both are finite, the system is SS.

is characterized by a checkerboard pattern consisting of an alternation of doubly filled sites and empty ones.

Figure 2 shows, for a fixed $V = 3$, the observables described in section 2.1 that we used to determine the various phases. The boson density as a function of the chemical potential displays clear plateaus, corresponding to gapped insulating phases (figure 2(a)). As mentioned above, jumps in figure 2(a) correspond to PS regions in figure 1. The structure factor and the SF stiffness are shown in figure 2(b). For low chemical potential (density), the system is in an SF state with non-zero SF stiffness and vanishing structure factor. At $\rho \approx 0.43$, the system phase separates and there are no values for these observables. At half filling, when the system moves to CDW I phase, the structure factor becomes finite. There is a small region, roughly around $0.5 < \rho < 0.51$, where the system is in an SS phase—here both the SF stiffness and the structure factor are non-zero. This phase is followed by a second region of PS that extends up to $\rho \approx 0.61$. At higher densities, an SF phase is observed up to unit filling, where an MI state follows, as revealed by vanishing SF density and structure factor.

3.1.2. Phase diagram at moderate on-site repulsion ($U = 5$). We now consider $U = 5$, a case of weaker repulsion that has not been studied earlier. For the moment, we still retain $T = 0$. The phase diagram figure 1(b) seems a bit simpler than for $U = 20$. Importantly, the particle-doped side now has to deal with much 'softer' bosons allowing for multiple occupancy on any given site (in the numerical calculations we allow for up to four bosons per site, which is sufficient for lattice fillings below unity). The hole-doped side is much less affected since the on-site repulsion has a lesser influence on lower densities. For weak NN repulsion V, the system stays SF across the entire range of densities from empty to unit filling and then goes into the MI state. At $V \approx 2.3$ up to 3.1, the system goes directly from an SF phase into an SS phase, which ends at a CDW II phase at unit filling. At larger V, a PS region appears. The biggest difference between $U = 20$ and 5 cases appears for higher values of V, where the PS region at the particle-doped side disappears and the SS phase occupies the entire region between the CDW I at half filling and the CDW II at unit filling.

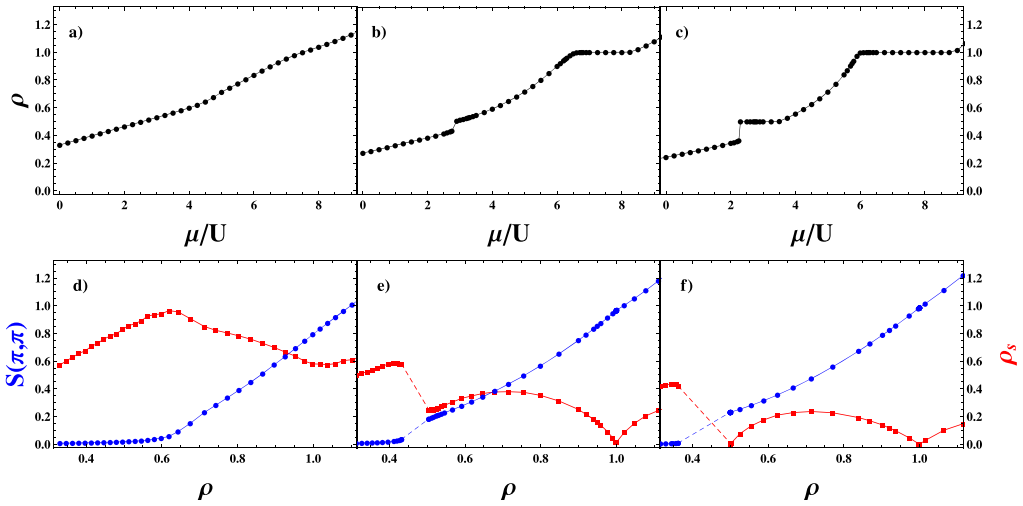

Figure 3. Top row: density versus chemical potential for $U = 5$ and different values of V: $V = 3.0$, 4.5 and 6.0 (left to right). The bottom row shows the corresponding structure factor (blue circles) and the SF stiffness (red squares).

The different transitions are revealed by slices through the phase diagram at fixed V (exemplified for a few values in figure 3). At $V = 3.0$, the density is strictly increasing across the entire range of μ (figure 3(a)). Notice, however, a change of the slope around $\mu/U = 4$, corresponding to $\rho = 0.6$. As seen in figure 3(d), the structure factor starts to rise in a similar parameter range, namely around $\rho = 0.65$. At the same time, the SF stiffness only has a peak at $\rho = 0.65$, but remains finite for all values of μ considered. Therefore, the increase of the structure factor is a clear sign of a second-order transition from an SF to an SS. Also, since the structure factor does not drop back to zero at $\rho = 1$, the unit-filling phase will be a CDW II and not an MI.

The next slice is taken at $V = 4.5$, where the state changes from SF to PS to SS without ever settling into the CDW I phase at half filling. In the density graph, figure 3(b), we can see a small jump that bypasses $\rho = \frac{1}{2}$. This explains why the CDW I phase does not appear at this value of V. The SF at small ρ is identified by a non-zero SF fraction and vanishing structure factor (figure 3(e)). This phase is followed by the PS region from $\rho \approx 0.435$ to 0.51. At higher densities, an SS state appears as characterized by non-zero structure factor and SF stiffness. Finally, the system settles into the CDW II state at unit filling.

The last slice at $V = 6.0$ is similar to the previous one at $V = 4.5$ with one major difference, the appearance of the CDW I phase at half filling. As before, we can see a jump (this time slightly larger) in the density, (figure 3(c)), but now it is followed by a plateau that signifies the CDW I phase. In figure 3(f), we see again the three distinct phases, SF up to $\rho \approx 0.35$, then a region of PS up to $\rho = 0.5$ and from half filling to unit filling there is the SS phase, once again ending in the CDW II state.

3.2. Phase diagrams at finite density-dependent tunneling

As we have seen in the previous section, the phase diagram of the EBHM at vanishing T displays a large variety of phases: MI, CDW, SF and SS. Additionally, there are various regions of PS,

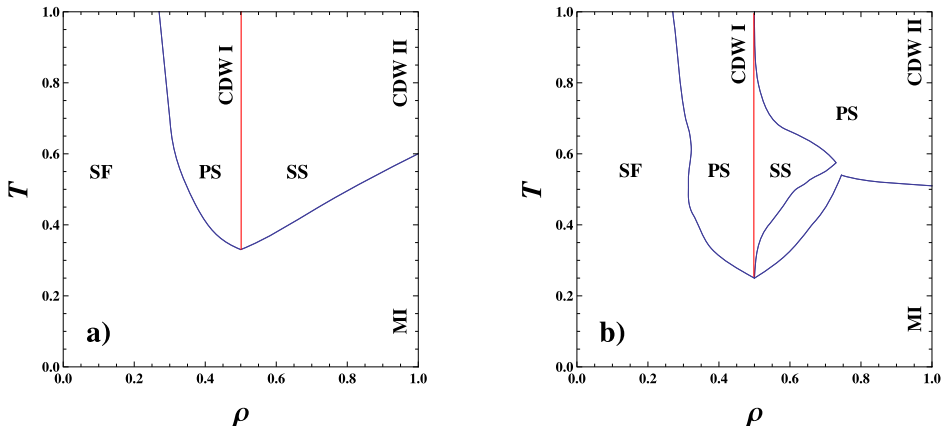

Figure 4. The phase diagrams for $U = 20$ at finite T (with $V = 10|T|$ and $t = 1$ the unit of energy). (a) If t and T are of the same sign, the relative importance of interactions decreases, leading to the disappearance of PS phases at greater-than-half filling. Compared to the $T = 0$ cases presented in figure 1, this phase diagram resembles more the case $U = 5$ than $U = 20$. (b) If T and t compete due to opposite signs, the relative importance of interactions is enhanced, increasing the PS regions. In fact, the two separate regions of PS in figure 1(b) increase to the point of overlapping.

some of which (the ones at filling larger than 1/2) disappear with decreasing on-site repulsion of the bosons. In this section, we study how this phase diagram of the usual EBHM is changed by the density-dependent hopping.

3.2.1. Phase diagram at strong on-site repulsion. The first case we study is $U = 20$ when the two tunneling amplitudes t and T have the same sign. Comparison of figure 4 with figure 2 shows that in the presence of density-dependent tunneling, the PS region at low V values has disappeared and there is no PS region between the SS and CDW II phases. One can explain this behavior by the increase in the total hopping due to the additional tunneling term T. Thus, the on-site repulsion U behaves as if it were effectively rescaled to a smaller value. Similar arguments explain the shift of the point where the $\rho = \frac{1}{2}$ plateau first appears and, therefore, the CDW I phase moves from $V \approx 2.5$ (with $T = 0$, figure 2) to $V \approx 3.5$ (figure 4). As a consequence, the phase diagram at $U = 20$, with t and T of the same sign, looks very similar to the one at $U = 5$ with vanishing T.

The behavior in the $U = 20$ phase diagram becomes more interesting when the two tunneling terms compete due to opposite signs, $T < 0$. The phase diagram is presented in figure 4(b). The CDW I phase now starts at a lower value of $|T|$ than in the previously discussed case. Similarly, the region of PS at the lower values of $|T|$ (and thus V) now becomes much larger. This shows that the system has a hardcore behavior for a larger range of parameters. Additionally, the SS region diminishes and finally disappears as V gets larger. These findings can be explained through the competition between t and T, which decreases the effective, overall tunneling strength. This decrease can alternatively be seen as an effective relative increase of the interaction parameters U and V. As a result, the hardcore behavior of the system becomes more pronounced and the PS regions become more important.

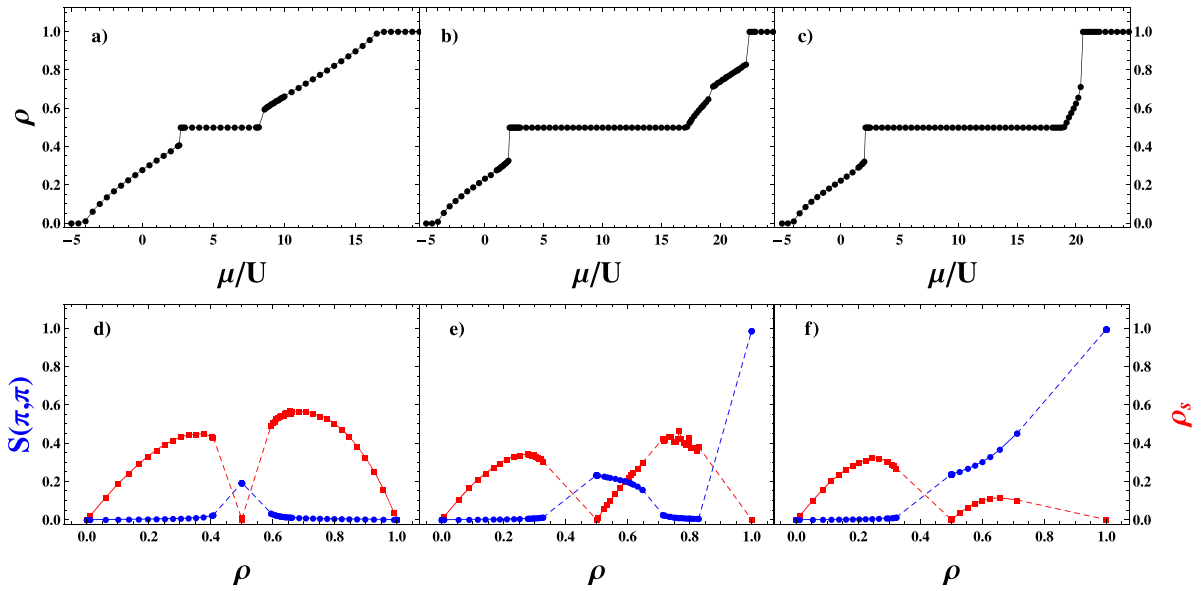

Figure 5. Density graphs of $U = 20$ for $T = -0.3$, -0.5 and -0.6 (left to right). Structure factor (blue circles) and SF stiffness (red squares) graphs for $U = 20$ at $T = 0.3$, 0.5 and 0.6 (left to right).

The observed phases may again be analyzed in detail via the cuts at fixed T (and therefore V) presented in figure 5. The first slice we present is for $T = -0.3$ ($V = 3.0$). As seen in figure 5(a), the plateau at half filling—a CDW I, as indicated by the finite structure factor, figure 5(d)—is surrounded by discontinuities in the density, thus implying regions of PS. These are surrounded by SF phases, with an MI appearing at unit filling.

The next slice cuts through the phase diagram at $T = -0.52$ ($V = 5.2$) and this time shows also a region of the SS phase for densities just above half filling (figure 5(e)). This SS may also be observed in the density plot, (figure 5(b)); above half filling, there is a small interval of steady increase before a discontinuity occurs around $\rho = 0.65$. After this PS region, there is a small region where the system becomes SF before once again phase separating. At unit filling, the system finally transitions into a CDW II phase. Below half filling, another jump in the density indicates yet another PS.

The final cut is taken at $T = -0.6$ ($V = 6.0$). Again, at low densities the system starts in an SF phase and then jumps through a region of PS to reach the CDW I phase at half filling. For higher densities, the system first enters an SS phase and around $\rho = 0.72$ a transition to PS occurs. This time, the system ends in the CDW II phase when unit filling is reached.

3.2.2. Moderate on-site repulsion ($U = 5$). In the previous section, we saw that the additional density-dependent tunneling term T can increase or decrease the effective importance of the interactions U and V, depending on whether it competes with or supports the single-particle tunneling t. In this section, we study this effect for weaker on-site interaction $U = 5$. The corresponding phase diagrams are presented in figure 6.

The positive T diagram reveals that the CDW I phase, present for $T = 0$, disappears completely (figure 6(a)). This means that at no point does there exist a plateau in the density

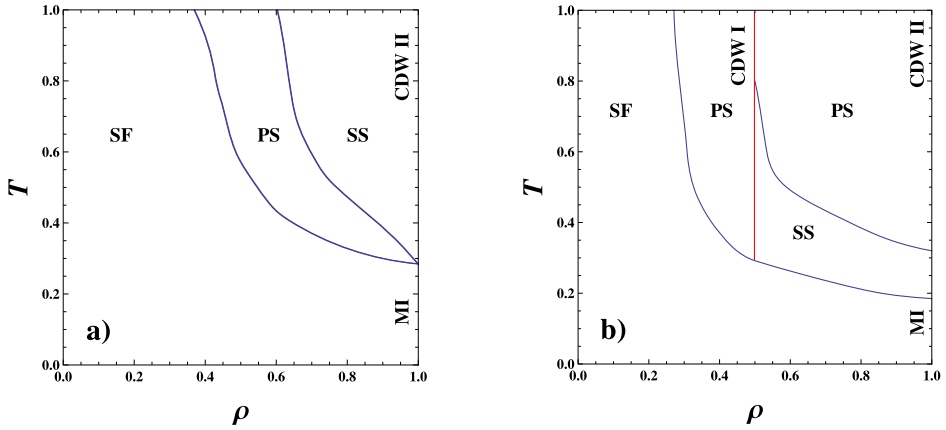

Figure 6. Phase diagrams for $U = 5$ and finite T. (a) If T and t have the same sign, the relative strength of tunneling is strongly increased with respect to the interactions. As a consequence, the CDW I phase has disappeared completely from this phase diagram. (b) When T and t are of opposite signs, the role of interactions is enhanced, leading to increased PS regions and again the CDW I phase is present.

graphs at $\rho = \frac{1}{2}$. Instead, a discontinuity bypasses half filling altogether. The rest of the behavior is rather similar to the system without the density-dependent term. There are still only three phases below unit filling, i.e. the SF phase at low densities and low T (and therefore at low V), the PS region near half filling for larger T and finally the SS phase for still higher T and larger densities. As can be expected, when the SF phase persists through the entire range of densities, the system ends in an MI state at unit filling. Instead, when the system at fixed T passes through the SS state, the final phase at unit filling is, as before, the CDW II phase.

Consider now the phase diagram of a system with $U = 5$ when the tunneling terms have opposite signs (figure 6(b)). Here, contrary to the case of positive T, the CDW I exists at half filling. This indicates that the relative importance of the effective total tunneling is suppressed for $T < 0$. Moreover, now a second region of PS appears above half filling. As a result, for $T \lesssim -0.8$ there is no stable phase with a density between the CDW I and the CDW II.

These observations about the phase diagram are supported by an analysis of cuts at a few chosen values of T (and thus V); see figure 7. At $T = -0.3$ ($V = 3.0$), one observes a smooth density increase all the way until unit filling, where a plateau appears (figure 7(a)). The structure factor starts increasing near half filling, indicating the transition from the SF to the SS phase (figure 7(d)); at unit filling, the system lands in the CDW II phase.

A cut at the slightly higher absolute value $T = -0.4$ ($V = 4.0$) reveals a plateau at half filling (CDW I) and a second one at unit filling (CDW II). Comparing the density plot (figure 7(b)) with those of SF stiffness and structure factor (figure 7(e)), we see that upon increasing the chemical potential, the SF phase appears at low densities, followed by the PS which transitions into the CDW I at half filling. For higher densities, there is a region of SS, where both the structure factor and the SF stiffness are non-zero. Finally, there is the jump caused by the PS region directly to the CDW II phase at unit filling.

Let us finally consider stronger density-dependent tunneling T and inter-site repulsion V, namely $T = -0.8$ ($V = 8.0$). Below half filling, the density gradually increases up to the value

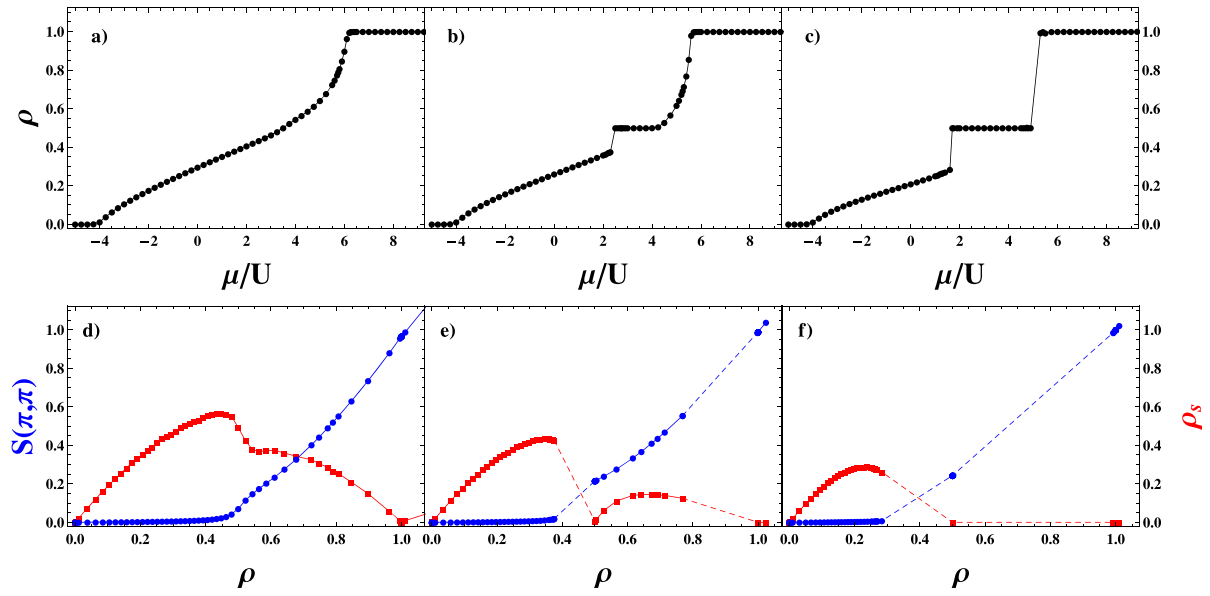

Figure 7. Top row: density graphs for $U = 5$ and $T = -0.3$, -0.4 and -0.8 (left to right). The bottom row shows the structure factor (blue circles) and the SF stiffness (red squares) for the same parameters.

of $\rho \approx 0.27$ and then jumps to the CDW I phase (figure 7(c)). After this phase, the density behaves step-like, jumping directly into the CDW II phase at $\rho = 1$. This behavior is seen clearly in the data presented in figure 7(f), where the SF phase for low densities is followed by two distinct regions of PS. These regions are only interrupted by the CDW I phase at half filling and the CDW II phase at full filling.

As these results show, for the lower on-site interaction $U = 5$, the density-dependent term T does not change much the overall behavior of the phase diagram if it has the same sign as the single-particle tunneling t. Instead, if the two tunneling terms have opposite signs, a large part of the SS phase disappears into a phase-separated region, due to the increased relative importance of the interaction terms.

4. Conclusions

In summary, we have studied the EBHM on a square lattice with additional terms coming from density-dependent tunneling. Taking these terms into account is relevant for experiments on ultracold dipolar molecules in optical lattices. The competition between the density-dependent tunneling, a standard single-particle hopping, finite on-site repulsion and nearest-neighbor repulsion gives rise to a rich phase diagram of the system.

Specifically, as has been found previously [8], at large on-site repulsion and without density-dependent tunneling, there are MI, CDW, SF and SS phases, as well as phase-separated parameter regions. Depending on the parameter strengths, this phase diagram undergoes considerable deformations. If we either reduce on-site repulsion or introduce density-dependent tunnelings that have the same sign as the single-particle hopping, some of the phase-separated regions disappear. Remarkably, if we introduce both of these effects simultaneously, the CDW

at half filling also disappears. In this case of same-sign tunnelings, both hopping processes act constructively, producing an effective larger tunneling, or respectively, weaker interactions.

We have also studied the phase diagram when the density-dependent tunneling and single-particle hopping compete due to their signs being opposite. Due to this competition, the relative importance of interaction terms is enhanced. In this case, the most striking effect is the disappearance of the SS into a phase-separated region. This occurs on the particle-doped side of the half filling CDW and at strong V.

Besides a theoretical interest in understanding how density-dependent tunneling terms change phase diagrams of EBHMs, our findings will help determine where one may expect exotic phases in experiments with ultracold dipolar molecules in optical lattices.

Acknowledgments

This work was supported by the International PhD Projects Programme of the Foundation for Polish Science within the European Regional Development Fund of the European Union, agreement no. MPD/2009/6. We acknowledge financial support from the Spanish Government grant TOQATA (FIS2008-01236) and Consolider Ingenio EU IP SIQS, ERC Advanced grant QUAGATUA, CatalunyaCaixa, Alexander von Humboldt Foundation and Hamburg Theory Award. MM and JZ thank Lluis Torner, Susana Horváth and all ICFO personnel for hospitality. OD and JZ acknowledge support from Polish National Center for Science project no. DEC-2012/04/A/ST2/00088. PH acknowledges support from the Austrian Science Fund (SFB F40 FOQUS) and the Marie Curie Initial Training Network COHERENCE.

References

[1] Lewenstein M, Sanpera A, Ahufinger V, Damski B, Sen(De) A and Sen U 2007 *Adv. Phys.* **56** 243
Lewenstein M, Sanpera A and Ahufinger V 2012 *Ultracold Atoms in Optical Lattices: Simulating Quantum Many-Body Systems* (Oxford: Oxford University Press)
[2] Bloch I, Dalibard J and Zwerger W 2008 *Rev. Mod. Phys.* **80** 885
[3] Jaksch D, Bruder C, Cirac J I, Gardiner C W and Zoller P 1998 *Phys. Rev. Lett.* **81** 3108
[4] Greiner M, Mandel O, Esslinger T, Hänsch T H and Bloch I 2002 *Nature* **415** 39–44
[5] Wessel S and Troyer M 2005 *Phys. Rev. Lett.* **95** 127205
[6] Heidarian D and Damle K 2005 *Phys. Rev. Lett.* **95** 127206
[7] Melko R G, Paramekanti A, Burkov A A, Vishwanath A, Sheng D N and Balents L 2005 *Phys. Rev. Lett.* **95** 127207
[8] Sengupta P, Pryadko L P, Alet F, Troyer M and Schmid G 2005 *Phys. Rev. Lett.* **94** 207202
[9] Batrouni G G, Hébert F and Scalettar R T 2006 *Phys. Rev. Lett.* **97** 087209
[10] Capogrosso-Sansone B, Trefzger C, Lewenstein M, Zoller P and Pupillo G 2010 *Phys. Rev. Lett.* **104** 125301
[11] Dalla Torre E G, Berg E and Altman E 2006 *Phys. Rev. Lett.* **97** 260401
[12] Hirsch J E 1989 *Physica* C **158** 326
[13] Dutta O, Eckardt A, Hauke P, Malomed B and Lewenstein M 2011 *New J. Phys.* **13** 023019
[14] Lühmann D S, Jurgensen O and Sengstock K 2012 *New J. Phys.* **14** 033021
[15] Łacki M, Delande D and Zakrzewski J 2013 *New J. Phys.* **15** 013062
[16] Bissbort U, Deuretzbacher F and Hofstetter W 2012 *Phys. Rev.* A **86** 023617
[17] Mering A and Fleischhauer M 2011 *Phys. Rev.* A **83** 063630
[18] Ospelkaus C, Ospelkaus S, Humbert L, Sengstock K and Bongs K 2006 *Phys. Rev. Lett.* **96** 020401
[19] Günter K, Stöferle T, Moritz H, Köhl M and Esslinger T 2006 *Phys. Rev. Lett.* **96** 180402

[20] Catani J, De Sarlo L, Barontini G, Minardi F and Inguscio M 2008 *Phys. Rev.* A **77** 011603
[21] Sowiński T, Dutta O, Hauke P, Tagliacozzo L and Lewenstein M 2012 *Phys. Rev. Lett.* **108** 115301
[22] Kim E and Chan M H W 2004 *Nature* **427** 225
[23] Kim E and Chan M H W 2004 *Science* **305** 1941
[24] Kim D Y and Chan M H W 2012 *Phys. Rev. Lett.* **109** 155301
[25] Kuklov A B, Prokof'ev N V and Svistunov B V 2011 *Physics* **4** 109
[26] Takekoshi T *et al* 2012 *Phys. Rev.* A **85** 032506
[27] Aikawa K, Akamatsu D, Hayashi M, Oasa K, Kobayashi J, Naidon P, Kishimoto T, Ueda M and Inouye S 2010 *Phys. Rev. Lett.* **105** 203001
[28] Bauer B *et al* 2011 *J. Stat. Mech.* P05001
[29] Bonnes L and Wessel S 2011 *Phys. Rev. Lett.* **106** 185302